

# History state formalism for time series with application to finance

F. Lomoc<sup>1</sup>, N. Canosa<sup>1</sup>, A.P. Boette<sup>1</sup>, R. Rossignoli<sup>1,2</sup>

<sup>1</sup> *Instituto de Física La Plata, CONICET, and Departamento de Física, Universidad Nacional de La Plata, C.C. 67, La Plata (1900), Argentina*

<sup>2</sup> *Comisión de Investigaciones Científicas (CIC), La Plata (1900), Argentina*

We present a method for analyzing general time series by employing the history state formalism of quantum mechanics. This formalism allows us to describe a complete evolution based on a single quantum state, the history state, which simultaneously includes -also as a quantum system- the reference clock. It naturally leads to the concept of system-time entanglement, with the ensuing entanglement entropy constituting a measure of the effective number of distinguishable states visited in the history. Through a quantum coherent state embedding of the time series data, it is then possible to associate a quantum history state to the series. The gaussian overlap between these coherent states provides thus a smooth measure of distinguishability between the series data. The eigenvalues of the corresponding overlap matrix determine in fact the entanglement spectrum and entropy of the history state, which provide a rigorous characterization of the evolution. As illustration, the formalism is applied to typical financial time-series data. Through the entanglement entropy and spectrum, different evolution regimes can be identified. Entanglement based volatility indicators are also derived, and compared with standard volatility measures.

## I. INTRODUCTION

Recent investigations in the area of Quantum Mechanics (QM) and Quantum Information have led to the development of the history state formalism [1–6], which incorporates time in an entirely quantum embedding. Starting from a relational state originally proposed by Page and Wootters [1], the formalism includes time through a reference clock, which is another quantum system itself, whose states serve as a time reference for the first system. Then the whole system can be described through a system-time history state, a joint quantum state of both the system and the clock, whose entanglement (“system-time entanglement”) indicates the “degree” of evolution of the system in time [5, 6]. Moreover, the system evolution equation itself, i.e., the Schrödinger equation, can also be derived from the joint history state, when forced to satisfy a proper “static” eigenvalue equation [1, 2, 6]. The formalism has recently gained attention in nonrelativistic QM [2–12], and has been also extended to the relativistic regime [13–17].

The aim of this work is to further this path, by studying time series from the perspective of the history state framework, where fully discrete formulations have also been considered [4–6, 11, 12]. We show that by associating the time series to a series of coherent quantum states, it is possible to define a particular history state, which describes important properties of the complete time series evolution. Its entanglement entropy is a measure of the number of effective orthogonal states visited during the evolution [5], then quantifying the degree of distinguishability of the set of values taken in the series. The more distinct the states are, i.e. the more variability is detected in the evolution, the more closely to orthogonal will the different states be, which translates into more entanglement between the system and the clock. The associated entanglement entropy depends in fact just on the overlaps between the states visited in the whole history,

i.e., on the eigenvalues of the ensuing overlap matrix, which determine the entanglement spectrum. As will be shown, this spectrum provides further insights for characterizing the evolution of the time series, supported by the rigorous perspective of majorization theory [18].

A fundamental aspect is that through the present coherent state quantum embedding of time series data (and a conveniently chosen scale factor), their basic gaussian nonorthogonality allows one to represent continuously the degree of distinguishability of data values, such that closely lying data whose difference is just barely relevant or slightly resolved correspond to states with high overlap. Hence, rather than a sharp cutoff, quantum states enable a consistent smooth transition between coincident and clearly distinguishable data. Moreover, through the Schmidt decomposition of the history state and the associated entanglement spectrum, the formalism provides a rigorous picture of the evolution in terms of a set of effective orthogonal states visited in the history and a concomitant set of positive probabilities or “occurrence frequencies”, which are just these eigenvalues. We note here that an arbitrary “overlap function” not based on true quantum states (i.e., on a true Gram or overlap matrix) does not ensure positive eigenvalues. On the other hand, a quantum embedding also allows in principle to quantum-simulate a time series, which opens the way to possible quantum computation [19] based schemes.

As specific application, we will consider the analysis through this formalism of financial time series. In recent decades, there has been a growing body of applications of mathematical and physical methods in the area of finance, leading to the establishment of what is called quantitative finance [20–28]. In addition, the interdisciplinary field called “Quantum Finance”, which merges methods and formalisms stemming from QM and quantitative finance, has provided a new perspective for the treatment of diverse problems in the area that has been receiving increasing attention [29–39].

Here we will examine well known financial time series. We start with the SPY, which is the ticker symbol for an ETF (Exchange-Traded Funds) that tracks the performance of the S&P500 (Standard and Poor's) index. The time series of the gold ETF (GLD) and Bitcoin (BTC) will be also considered. By means of the system-time entanglement entropy and spectrum, we will characterize different regimes of prices along the evolution. Besides, we will derive measures that are able to recognize the variability of the asset prices and that can be interpreted as proxies of their volatility. They will be compared with standard volatility measures for these assets, namely the volatility index (VIX) [41] for the SPY and GLD, and the Crypto Volatility Index (CVI) [42] for Bitcoin.

We first review in sections II A–II C the history state formalism, including the concept of system-time entanglement entropy and its relation with mutual information, while generalized entropies, their relation with majorization theory and their application to the characterization of different evolution regimes of entanglement entropies, are described in II D. In II E–II F we introduce the history state formalism for time series through the quantum coherent state embedding of the time series data, and the ensuing gaussian overlap. Finally, in section III we illustrate the formalism through its application to financial time series for the above mentioned assets, where different types of history states are analyzed. Conclusions are drawn in IV. App. A contains the essential elements of majorization theory and related demonstrations of results in II D, while App. B provides a summary of the main features of volatility measures.

## II. FORMALISM

### A. Discrete history state formalism in QM

We consider a quantum system  $S$  whose states  $|\psi\rangle$  belong to a Hilbert space  $\mathcal{H}_S$ , and a reference clock system  $T$  with Hilbert space  $\mathcal{H}_T$ . If  $|\psi_n\rangle \in \mathcal{H}_S$  is the state of  $S$  when the clock is in state  $|n\rangle \in \mathcal{H}_T$ , the history state  $|\Psi\rangle \in \mathcal{H}_S \otimes \mathcal{H}_T$  over  $N$  distinguishable ‘times’  $|n\rangle$ ,  $n = 0, \dots, N-1$ ,  $\langle n|n'\rangle = \delta_{nn'}$ , is

$$|\Psi\rangle = \frac{1}{\sqrt{N}} \sum_{n=0}^{N-1} |\psi_n\rangle \otimes |n\rangle. \quad (1)$$

It describes the whole evolution of  $S$  along the chosen set of  $N$  times. The states  $|\psi_n\rangle$  are normalized but obviously not necessarily orthogonal, and can be recovered from  $|\Psi\rangle$  as  $|\psi_n\rangle = \sqrt{N} \langle n|\Psi\rangle$ , where the ‘partial’ product is defined through  $\langle n|(|\psi_S\rangle \otimes |\phi_T\rangle) = \langle n|\phi_T\rangle |\psi_S\rangle$ .

All information about the system evolution can then be retrieved from  $|\Psi\rangle$ . In particular, time averages of system  $S$  observables  $O_S$ , defined as

$$\langle O_S \rangle_N = \frac{1}{N} \sum_{n=0}^{N-1} \langle \psi_n | O_S | \psi_n \rangle, \quad (2)$$

which in principle require averages (and hence measurements) at each time  $n$ , can be directly obtained as

$$\langle O_S \rangle_N = \langle \Psi | \mathcal{O}_S | \Psi \rangle, \quad (3)$$

where  $\mathcal{O}_S = O_S \otimes \mathbb{1}_N$  and  $\mathbb{1}_N = \sum_{n=0}^{N-1} |n\rangle \langle n|$  is the orthogonal projector onto the subspace of  $\mathcal{H}_T$  spanned by the  $N$  clock states  $|n\rangle$ , such that  $\langle n | \mathcal{O}_S | n' \rangle = O_S \delta_{nn'}$ . Thus, a realization of  $|\Psi\rangle$  enables an efficient evaluation of time averages as a single expectation value (3).

We can always consider the normalized states  $|\psi_n\rangle$  as emerging from an initial state  $|\psi_0\rangle$  through a unitary evolution,

$$|\psi_n\rangle = U_n |\psi_0\rangle, \quad (4)$$

with  $U_n^\dagger U_n = \mathbb{1}_S$  and  $U_0 = \mathbb{1}_S$ . Then we can define a cyclic system-clock translation superoperator

$$\mathcal{U} = \sum_{n=1}^N U_{n,n-1} \otimes |n\rangle \langle n-1|, \quad (5)$$

over  $\mathcal{H}_S \otimes \mathcal{H}_T$ , where  $U_{n,n-1} = U_n U_{n-1}^\dagger$  and  $U_N \equiv U_0$ ,  $|N\rangle \equiv |0\rangle$ , such that  $\mathcal{U}^\dagger \mathcal{U} = \mathbb{1}_S \otimes \mathbb{1}_N$ . Since  $\mathcal{U}(|\psi_{n-1}\rangle \otimes |n-1\rangle) = |\psi_n\rangle \otimes |n\rangle \forall n$ , the history state (1) satisfies

$$\mathcal{U}|\Psi\rangle = |\Psi\rangle, \quad (6)$$

i.e. it is an exact eigenstate of  $\mathcal{U}$  with eigenvalue 1, thus remaining fully invariant under  $\mathcal{U}$ .

Conversely, Eq. (6), which can be considered as a discrete version of a Wheeler-DeWitt-type equation [43], implies that  $|\Psi\rangle$  is necessarily a history state of the form (1), with  $|\psi_n\rangle = U_n |\psi_0\rangle$  undergoing a unitary stepwise evolution and  $|\psi_0\rangle$  an *arbitrary* normalized initial state: Eqs. (5)–(6) entail that just the  $N$  times  $|n\rangle$  enter in the support of  $|\Psi\rangle$ , such that  $|\Psi\rangle = \sum_n \langle n|\Psi\rangle \otimes |n\rangle$ , then having the form (1) for  $|\psi_n\rangle = \sqrt{N} \langle n|\Psi\rangle$ , with  $\langle n|\Psi\rangle = \langle n|\mathcal{U}|\Psi\rangle = U_{n,n-1} \langle n-1|\Psi\rangle$ , i.e.,  $|\psi_n\rangle = U_{n,n-1} |\psi_{n-1}\rangle = U_n |\psi_0\rangle$ , and  $\langle \Psi|\Psi\rangle = \frac{1}{N} \sum_n \langle \psi_n|\psi_n\rangle = \langle \psi_0|\psi_0\rangle = 1$  if  $|\Psi\rangle$  is assumed normalized. Thus, unitary stepwise evolution of system  $S$  states  $\propto \langle n|\Psi\rangle$  directly follows from Eqs. (5)–(6) [5, 6].

The history state can itself be generated from an initial seed state  $|\psi_0\rangle \otimes |0\rangle$  through a unitary quantum gate  $\mathcal{W}$ ,

$$|\Psi\rangle = \mathcal{W}(|\psi_0\rangle \otimes |0\rangle), \quad (7)$$

where  $\mathcal{W} = (\sum_n U_n \otimes |n\rangle \langle n|) (\mathbb{1}_S \otimes H_N)$ . Here  $H_N$  is a Hadamard-like local operator on  $\mathcal{H}_T$  satisfying  $H_N|0\rangle = \frac{1}{\sqrt{N}} \sum_n |n\rangle$ , whereas  $\sum_n U_n \otimes |n\rangle \langle n|$  is a control-like operator on  $\mathcal{H}_S \otimes \mathcal{H}_T$ . A simulation over  $N = 2^m$  times can be efficiently achieved with just  $m$  qubits, in which case  $H_N = H^{\otimes m}$  [5, 6].

### B. System-time entanglement as quantifier of evolution

The history state (1) is in general an *entangled* state, i.e., it is not a product state  $|\psi\rangle_S \otimes |\phi\rangle_T$ . The only exception is the case of *stationary* system states, i.e. states

which evolve just with a phase,  $|\psi_n\rangle = e^{-i\phi_n}|\psi_0\rangle \forall n$ , with  $\phi_n$  real, for which it becomes *separable*:  $|\Psi\rangle = |\psi_0\rangle \otimes |\phi\rangle_T$ , with  $|\phi\rangle_T = \frac{1}{\sqrt{N}} \sum_n e^{-i\phi_n}|n\rangle$  a superposition of all time states  $|n\rangle$ . In this case there is no entanglement between  $S$  and the clock  $T$ , i.e., between ‘‘system and time’’.

The opposite limit is that in which the system evolves into a new orthogonal state at each step, such that  $\langle\psi_n|\psi_{n'}\rangle = \delta_{nn'} \forall n, n'$ . In this case  $|\Psi\rangle$  becomes *maximally entangled*, with (1) becoming its Schmidt decomposition. Therefore, its ‘‘degree of entanglement’’, i.e. of the system-time entanglement, is a measure of the distinguishable evolution of the system  $S$  along the  $N$  times.

We now recall that bipartite pure state entanglement can be measured through the entanglement entropy,

$$E(S, T) = S(\rho_S) = S(\rho_T), \quad (8)$$

where  $\rho_{S(T)}$  are the reduced states of  $S$  ( $T$ ),

$$\rho_S = \text{Tr}_T |\Psi\rangle\langle\Psi| = \frac{1}{N} \sum_n |\psi_n\rangle\langle\psi_n|, \quad (9a)$$

$$\rho_T = \text{Tr}_S |\Psi\rangle\langle\Psi| = \frac{1}{N} \sum_{n, n'} \langle\psi_{n'}|\psi_n\rangle |n\rangle\langle n'|, \quad (9b)$$

with  $\text{Tr}_{T(S)}$  denoting the partial trace, which are *isospectral*, i.e., they have the same nonzero eigenvalues and hence the same entropy. This set of eigenvalues is the *entanglement spectrum*. The entropy in (8) will be first chosen as the von Neumann entropy

$$S(\rho) = -\text{Tr} \rho \log \rho. \quad (10)$$

Explicitly, we see from Eq. (9b) that the eigenvalues of  $\rho_T$  are just those of the *normalized overlap matrix*  $\mathbf{O}_N$  of the system states  $|\psi_n\rangle$ , of elements

$$(\mathbf{O}_N)_{n'n} = \langle n|\rho_T|n'\rangle = \langle\psi_{n'}|\psi_n\rangle/N, \quad (11)$$

which is hermitian and positive semidefinite, satisfying  $\text{Tr} \mathbf{O}_N = 1$ . Since it is the Gram matrix of the states  $|\psi_n\rangle/\sqrt{N}$ , its rank  $N_s$ , i.e., the number of nonzero eigenvalues, is just *the number of linearly independent system states  $|\psi_n\rangle$  involved in the discrete evolution, i.e., the dimension of the subspace  $\mathcal{S} \subset \mathcal{H}_S$  spanned by the  $N$  states  $|\psi_n\rangle$* . If  $\mathbf{W}$  is the unitary matrix diagonalizing  $\mathbf{O}_N$ ,

$$(\mathbf{W}^\dagger \mathbf{O}_N \mathbf{W})_{kk'} = \lambda_k \delta_{kk'}, \quad (12)$$

with  $\lambda_k \geq 0$ ,  $\sum_k \lambda_k = 1$ , we may rewrite the history state (1) and the densities (9a)–(9b) in the diagonal forms

$$|\Psi\rangle = \sum_{k=1}^{N_s} \sqrt{\lambda_k} |k\rangle_S \otimes |k\rangle_T, \quad (13)$$

$$\rho_S = \sum_{k=1}^{N_s} \lambda_k |k\rangle_S \langle k|, \quad \rho_T = \sum_{k=1}^{N_s} \lambda_k |k\rangle_T \langle k|, \quad (14)$$

where sums run just over the  $N_s$  non-zero eigenvalues  $\lambda_k > 0$  of  $\mathbf{O}_N$  and

$$|k\rangle_S = \frac{1}{\sqrt{N\lambda_k}} \sum_n W_{nk} |\psi_n\rangle, \quad |k\rangle_T = \sum_n W_{nk}^* |n\rangle, \quad (15)$$

are *orthogonal* states of  $S$  and  $T$ :  ${}_S\langle k'|k\rangle_S = \delta_{kk'}$  for  $k \leq N_s$ ,  ${}_T\langle k|k'\rangle_T = \delta_{kk'}$  for  $k \leq N$ . Eq. (13) is precisely the *Schmidt decomposition* of  $|\Psi\rangle$ .

The entropy (8) can then be explicitly written as

$$E(S, T) = -\sum_{k=1}^{N_s} \lambda_k \log \lambda_k, \quad (16)$$

satisfying  $0 \leq E(S, T) \leq \log N$ . The lower limit is reached in the stationary case  $N_s = 1$ , where  $\rho_S = |\psi_0\rangle\langle\psi_0|$ ,  $\rho_T = |\phi\rangle_T\langle\phi|$  are pure and hence  $S(\rho_S) = S(\rho_T) = 0$ , and the upper limit in the maximally evolving case  $N_s = N$  and  $\lambda_k = 1/N \forall k$ , where  $\rho_S = \Pi_S/N$ ,  $\rho_T = \mathbb{1}_N/N$  are maximally mixed, with  $\Pi_S$  the orthogonal projector on the subspace spanned by the  $N$  orthogonal states  $|\psi_n\rangle$ , and hence  $S(\rho_S) = S(\rho_T) = \log N$ .

Thus, using  $\log \equiv \log_2$ , we may approximately consider

$$N_E = 2^{E(S, T)}, \quad (17)$$

as the *effective* number of orthogonal states visited in the evolution along the  $N$  times. It is 1 in the separable case  $E(S, T) = 0$  and  $N$  in the maximally evolving case  $E(S, T) = \log_2 N$ , lying otherwise in the interval  $(1, N)$ .

The effective number (17) takes into account the relative frequency with which distinct states appear. Hence, it is lower than the rank  $N_s$  of the overlap matrix, which just counts the number of linearly independent states of the history regardless of their relative frequencies.

For example, if just  $M \leq N$  strictly orthogonal states  $|\tilde{\psi}_m\rangle$  are visited in the  $N$  times history, each  $l_m$  times with  $\sum_{m=1}^M l_m = N$ , the history state (1) becomes

$$|\Psi\rangle = \sum_{m=1}^M \sqrt{p_m} |\tilde{\psi}_m\rangle \otimes |\tilde{m}\rangle, \quad (18)$$

with  $p_m = l_m/N$  ( $\sum_m p_m = 1$ ),  $\langle\tilde{\psi}_{m'}|\tilde{\psi}_m\rangle = \delta_{mm'}$  and  $|\tilde{m}\rangle = \frac{1}{\sqrt{l_m}} \sum_n |n\rangle \langle\psi_m|\psi_n\rangle$  normalized orthogonal clock states. In this case Eq. (18) is already the Schmidt decomposition (13), i.e.  $\lambda_k = p_m$  in (16). Then Eq. (17) yields  $N_E \leq M$ , with  $N_E = M$  iff all  $l_m$  are equal, i.e. if all  $M$  orthogonal states are visited the same number of times, such that  $l_m = N/M$  and  $p_m = 1/M \forall m$ , implying  $E(S, T) = \log M$ . Otherwise,  $E(S, T)$  and hence  $N_E$  are smaller, the minimum reached when just one of the  $M$  orthogonal states appears more than once ( $p_m = \frac{N-M+1}{N}$  for this state,  $p_m = \frac{1}{N}$  for the rest).

So far we have implicitly assumed  $\dim \mathcal{H}_T \geq N$ , the formalism valid for *any* dimension  $d_S$  of  $\mathcal{H}_S$  (finite or infinite). Nonetheless, if  $d_S < N$ , the rank  $N_s$  obviously satisfies  $N_s \leq d_S < N$ , and it is more convenient to

write  $|\psi_n\rangle = \sum_i C_{in}|i\rangle$ , with  $\{|i\rangle\}$  any orthogonal basis of  $\mathcal{H}_S$  and  $C_{in} = \langle i|\psi_n\rangle$ . Then the  $N \times N$  overlap matrix  $\mathbf{O} = C^\dagger C/N$  will have the same nonzero eigenvalues as the smaller  $d_S \times d_S$  matrix  $CC^\dagger/N$ , which is thus more convenient. The Schmidt decomposition (13) can then be obtained from the singular value decomposition of  $C$ , with  $\lambda_k$  the square of its singular values  $\sigma_k$ .

### C. Entanglement entropy and mutual information

The entanglement entropy (16) also admits other interpretations. Let us first recall that the mutual information of a bipartite system  $A + B$  is defined as

$$I(A, B) = S(A) + S(B) - S(A, B), \quad (19)$$

$$= S(A) - S(A|B), \quad (20)$$

where  $S(A|B) = S(A, B) - S(B)$  is the conditional entropy and in the quantum case,  $S(A) = S(\rho_A)$ ,  $S(B) = S(\rho_B)$  and  $S(A, B) = S(\rho_{AB})$ , with  $\rho_{A(B)} = \text{Tr}_{B(A)} \rho_{AB}$  the reduced density operator of  $A$  ( $B$ ). Eq. (19) is a measure of the total (classical plus quantum) correlations in the system, satisfying  $I(A, B) \geq 0$ , with  $I(A, B) = 0$  iff  $\rho_{AB} = \rho_A \otimes \rho_B$ .

For a pure quantum state  $\rho_{AB} = |\Psi\rangle\langle\Psi|$ ,  $S(\rho_{AB}) = 0$  while  $S(A) = S(B) = E(A, B)$ , with  $E(A, B)$  the entanglement entropy (i.e., Eq. (8) in the case of the history state), such that  $I(A, B) = 2E(A, B)$ . Thus, in pure entangled states it exceeds the classical upper bound  $I(A, B) \leq S(A)$  valid for any classical joint random variable (for which  $S(A|B) = \sum_j S(A|j)p(B=j) \geq 0$ ), since entanglement leads to  $S(A|B) = -S(A) < 0$ .

Let us now suppose that some decoherence process takes place such that the coherence of the pure history state (1) is lost and one is left with the decohered *classically correlated state*

$$\rho'_{ST} = \sum_n \Pi_n \rho_{ST} \Pi_n = \frac{1}{N} \sum_n |\psi_n\rangle\langle\psi_n| \otimes |n\rangle\langle n|, \quad (21)$$

where  $\Pi_n = \mathbb{1}_S \otimes |n\rangle\langle n|$  are the orthogonal projectors on the clock states  $|n\rangle$ . For example, a local projective measurement in the clock basis  $\{|n\rangle\}$  (without postselection) leads to the postmeasurement state (21). This state is a mixture of product states and hence it is *separable* (in the sense that it can be generated by LOCC), having no entanglement:  $E'(S, T) = 0$ .

Nonetheless, the previous entanglement entropy (16) reemerges exactly in (21) as *mutual information*, now measuring the classical correlation between  $S$  and  $T$ : In the state (21) we obtain

$$I'(S, T) = S(\rho'_S) + S(\rho'_T) - S(\rho'_{ST}) \quad (22)$$

$$= S(\rho_S) = E(S, T), \quad (23)$$

with  $E(S, T)$  the original system-time entanglement entropy (8), since  $\rho'_S = \frac{1}{N} \sum_n |\psi_n\rangle\langle\psi_n| = \rho_S$ , Eq. (9a) (in agreement with the general no signaling result that a

local measurement at  $T$  with no postselection cannot affect the reduced density of  $S$ ), while  $\rho'_T = \frac{1}{N} \sum_n |n\rangle\langle n|$  is isospectral with  $\rho'_{ST}$  and hence  $S(\rho'_S) = S(\rho'_{ST})$ , i.e.,  $S(S|T) = 0$ . The latter vanishes as the conditional states of  $S$ ,  $\langle n|\rho'_{ST}|n\rangle \propto |\psi_n\rangle\langle\psi_n|$ , are pure  $\forall |n\rangle$ .

Hence, we can again measure the effective number of orthogonal states visited in the now classically correlated mixed history state (21) through essentially the same quantity  $S(\rho_S)$ , now equal to  $I'(S, T)$ .

Remarkably, the same value of  $I'(S, T)$  is obtained if the decoherence or local measurement takes place in *any* other orthogonal clock basis  $\{|j\rangle\}$  of  $T$ ,  $\langle j|\tilde{j}'\rangle = \delta_{jj'}$ : The history state (1) can be rewritten in this clock basis as

$$|\Psi\rangle = \sum_j \sqrt{p_j} |\phi_j\rangle \otimes |\tilde{j}\rangle, \quad (24)$$

where  $|\phi_j\rangle = \sum_n \langle \tilde{j}|n\rangle |\psi_n\rangle / \sqrt{p_j} \propto \langle j|\Psi\rangle$  are normalized conditional system states and  $p_j = (\mathbf{V}^\dagger \mathbf{O}_N \mathbf{V})_{jj} \geq 0$ , with  $\mathbf{O}$  the matrix (11) and  $\mathbf{V}$  the unitary matrix of elements  $V_{nj} = \langle n|j\rangle$  ( $\sum_j p_j = 1$ ). Hence, after decoherence or a local measurement at the clock in this basis, we obtain

$$\tilde{\rho}'_{ST} = \sum_j \tilde{\Pi}_j \rho_{ST} \tilde{\Pi}_j = \sum_j p_j |\phi_j\rangle\langle\phi_j| \otimes |\tilde{j}\rangle\langle\tilde{j}|, \quad (25)$$

where  $\tilde{\Pi}_j = \mathbb{1}_S \otimes |\tilde{j}\rangle\langle\tilde{j}|$ . Again  $\tilde{\rho}'_S = \text{Tr}_T \tilde{\rho}'_{ST} = \sum_j p_j |\phi_j\rangle\langle\phi_j| = \rho_S$ , Eq. (9a), in agreement with no signaling, while  $\tilde{\rho}'_T = \sum_j p_j |\tilde{j}\rangle\langle\tilde{j}|$  remains isospectral with  $\tilde{\rho}'_{ST}$ , such that  $S(S|T) = 0$  (as  $\langle \tilde{j}|\tilde{\rho}'_{ST}|\tilde{j}\rangle \propto |\phi_j\rangle\langle\phi_j|$  remains pure  $\forall j$ ). Therefore, we still obtain

$$\begin{aligned} \tilde{I}'(S, T) &= S(\tilde{\rho}'_S) + S(\tilde{\rho}'_T) - S(\tilde{\rho}'_{ST}) \\ &= S(\rho_S) = E(S, T). \end{aligned} \quad (26)$$

In summary,  $E(S, T)$  can also be considered as the *mutual information* of the decohered classically correlated mixed state which follows after an unread complete local measurement at the clock in an arbitrary basis.

### D. Generalized entropies and majorization based characterization of evolution

Other entropies can also be considered in Eq. (8). In particular, the Renyi entropies [44]

$$S_q^R(\rho) = \frac{1}{1-q} \log \text{Tr} \rho^q, \quad q > 0, \quad (27)$$

approach the von Neumann entropy (10) for  $q \rightarrow 1$  and attain the same previous lower and upper limits  $\forall q > 0$ :  $S_q^R(\rho) = 0$  for  $\rho$  pure ( $\rho^2 = \rho$ ),  $S_q^R(\rho) = \log N$  for  $\rho$  maximally mixed ( $\rho = \mathbb{1}/N$ ,  $N = \text{Tr} \mathbb{1}$ ), such that  $0 \leq S_q^R(\rho) \leq \log N$ . The ensuing entanglement entropy is

$$E_q(S, T) = S_q^R(\rho_S) = S_q^R(\rho_T) = \frac{1}{1-q} \log \sum_k \lambda_k^q, \quad (28)$$

and the associated number of effective states visited is again  $N_{E_q} = 2^{E_q(S,T)}$  for  $\log = \log_2$ . For  $q \rightarrow 1$ ,  $E_q(S,T) \rightarrow E(S,T)$ . The  $q = 2$  case,

$$S_2^R(\rho) = -\log \text{Tr} \rho^2, \quad (29)$$

is particularly convenient as it just depends on the purity  $\text{Tr} \rho^2$  and does not require the calculation of the eigenvalues of  $\rho$ . The associated entanglement entropy can then be directly expressed in terms of the overlap matrix  $\mathbf{O}_N$ :

$$\begin{aligned} E_2(S,T) &= S_2^R(\rho_{T(S)}) = -\log \text{Tr} \mathbf{O}_N^2 \\ &= -\log \left( \frac{1}{N^2} \sum_{n,n'} |\langle \psi_n | \psi_{n'} \rangle|^2 \right). \end{aligned} \quad (30)$$

Trace-form entropies [45]  $S_f(\rho) = \text{Tr} f(\rho)$ , where  $f: [0, 1] \rightarrow \mathbb{R}$  is a strictly concave function satisfying  $f(0) = f(1) = 0$  (and hence  $f(\lambda) > 0 \forall \lambda \in (0, 1)$ ), could also be employed in (8). In particular, for  $f(\rho) = \frac{1}{q-1}(\rho - \rho^q)$ , we obtain the Tsallis entropies [46]  $S_q(\rho) = \frac{1}{q-1}(1 - \text{Tr} \rho^q)$ ,  $q > 0$ , which also reduce to the von Neumann entropy for  $q \rightarrow 1$  and relate to the Renyi entropies through  $S_q^R = \frac{1}{1-q} \log[1 - (q-1)S_q]$ . The latter is just an increasing function of  $S_q$  for  $q > 0$ .

These trace form entropies are concave functions of  $\rho$  and satisfy (under the previous conditions for  $f$ ) the fundamental inequality

$$S_f(\rho) \geq S_f(\rho') \quad \text{if } \rho \prec \rho', \quad (31)$$

i.e. if  $\rho$  is *majorized* by  $\rho'$  [47, 48], a condition involving all partial sums of the eigenvalues of  $\rho, \rho'$  (see App. A):

$$\rho \prec \rho' \iff \sum_{k=1}^l \lambda_k \leq \sum_{k=1}^l \lambda'_k, \quad l = 1, \dots, n-1, \quad (32)$$

where  $\lambda_k, \lambda'_k$  denote the eigenvalues of  $\rho$  and  $\rho'$  respectively, sorted in *decreasing* order ( $\lambda_{k+1} \leq \lambda_k \forall k$ ) and  $n$  is the dimension of  $\rho$  and  $\rho'$  (equality  $\text{Tr} \rho = \text{Tr} \rho' = 1$  is assumed for  $l = n$ ). Eq. (31) is actually satisfied by all Schur-concave functions of  $\rho$  [18], which include all Renyi entropies (27) for  $q > 0$ .

Thus, majorization implies an universal entropy increase, being a more stringent criterion for mixedness or disorder than an entropy increase for a single choice of entropic function. Conversely, while  $S_f(\rho) \geq S_f(\rho')$  for a single choice of  $f$  does not imply majorization, the converse relation *does hold* if valid for *all* concave  $f$ :  $S_f(\rho) \geq S_f(\rho') \forall S_f \iff \rho \prec \rho'$  [49].

When applied to the history state, Eqs. (31)–(32) allow us to identify three distinct evolution regimes when considering the system-time entanglement entropy as a function of the number  $N$  of times of the history. Denoting with  $\rho_{S(T)}^{(N)}$  the reduced states of  $S$  and  $T$  in the history up to time  $N$ , we obtain:

I. *Universal system-time entanglement entropy increase*: It arises if

$$\rho_{T(S)}^{(N+1)} \prec \rho_{T(S)}^{(N)}, \quad (33)$$

i.e., when  $\rho_{S(T)}^{(N+1)}$  is *majorized* by  $\rho_{S(T)}^{(N)}$ . This ensures that

$$E_f^{(N+1)}(S,T) \geq E_f^{(N)}(S,T) \quad (34)$$

for *any* choice of entropy (i.e., of Schur-concave function of  $\rho_{S(T)}$ ), including von Neumann, Renyi and all trace-form entanglement entropies  $E_f(S,T) = S_f(\rho_{S(T)})$ .

A related basic fundamental result is the following:

*Lemma 1.* Eq. (33) is satisfied whenever a state  $|\psi_n\rangle$  orthogonal to all previous states,  $\langle \psi_{n'} | \psi_n \rangle = 0 \forall n' < n$ , is added to the history at step  $n = N$  (sufficient condition).

The proof is straightforward: If  $\boldsymbol{\lambda}^{(N)} = \{\lambda_k^{(N)}\}$  are the eigenvalues of  $\mathbf{O}_N$  for the  $N$ -times history, those of  $\mathbf{O}_{N+1}$  after such addition are  $\boldsymbol{\lambda}^{(N+1)} = \{\frac{N}{N+1}\lambda_k^{(N)}\} \cup \{\frac{1}{N+1}\}$ , due to the orthogonality of the added state. It is then easily verified (see App. A) that

$$\boldsymbol{\lambda}^{(N+1)} \prec \boldsymbol{\lambda}^{(N)}, \quad (35)$$

implying Eqs. (33)–(34). Therefore, by continuity, the regime (33)–(34) arises for some interval of values of  $N$  essentially when the system visits a sufficiently distinguishable new state at each step of this interval.

II. *Universal system-time entanglement entropy decrease*: It arises if

$$\rho_{T(S)}^{(N)} \prec \rho_{T(S)}^{(N+1)}, \quad (36)$$

i.e., when  $\rho_{S(T)}^{(N+1)}$  *majorizes*  $\rho_{S(T)}^{(N)}$ . This implies

$$E_f^{(N+1)}(S,T) \leq E_f^{(N)}(S,T) \quad (37)$$

for *any* choice of entropy.

This is a very special case which requires, as necessary (but not sufficient) condition that the state added at the last step is already contained in the history, such that just a null eigenvalue of  $\mathbf{O}_N$  is added. Otherwise the last majorization inequality cannot be fulfilled.

In addition, the state added should be essentially among the most visited in the previous history, since otherwise it could increase the weight of a seldom visited state, leveling the distribution and hence preventing this inverse majorization.

For instance, let us consider a sequence where one state  $|\psi\rangle$  which is orthogonal to all other states of the history occurs  $M < N$  times, then leading to an eigenvalue  $M/N$  of  $\mathbf{O}_N$  which we assume is the largest. If  $\tilde{\boldsymbol{\lambda}}^{(N-M)}$  denotes the spectrum of the overlap matrix of the remaining  $N - M$  states, the sorted spectrum of  $\mathbf{O}_N$  is  $\boldsymbol{\lambda}^{(N)} = (\frac{M}{N}, \frac{\tilde{\lambda}^{(N-M)}}{N})$ , with  $\tilde{\lambda}_{\max}^{(N-M)} \leq M$ . Then further addition of the same  $|\psi\rangle$  leads to a spectrum  $\boldsymbol{\lambda}^{(N+1)} = (\frac{M+1}{N+1}, \frac{\tilde{\lambda}^{(N-M)}}{N+1})$ . It is easily verified that  $\boldsymbol{\lambda}^{(N)} \prec \boldsymbol{\lambda}^{(N+1)}$ , since their partial sums satisfy  $S_j^{(N)} = \frac{M+\tilde{S}_j^{(N-M)}}{N} \leq S_j^{(N+1)} = \frac{M+1+\tilde{S}_j^{(N-M)}}{N+1}$ , as  $M + \tilde{S}_j^{(N-M)} \leq N$  for  $j \leq N - M$ , thus leading to (36).

If the last added state does not coincide exactly with  $|\psi\rangle$  but is sufficiently close, by continuity this regime will

occur approximately since the last eigenvalue added, if not zero, will be very small.

III. *Non-universal regime*: Here Eq. (33) does not hold in any direction ( $\rho^{(N+1)} \not\prec \rho^{(N)}$  and  $\rho^{(N)} \not\prec \rho^{(N+1)}$ ), implying that some entanglement entropies will increase but others will decrease at the  $N + 1$  step. For example, one could stick to the von Neumann entropy and use just the associated entanglement entropy (8)–(10) as measure ( $q \rightarrow 1$  in the Renyi case), but this does not ensure that other choices of entropy will exhibit the same behavior.

It should be here noticed that conversion of a single entangled pure bipartite state  $|\Psi\rangle$  by LOCC (local operations and classical communication) into  $|\Phi\rangle$  requires majorization of the associated reduced densities (and not just  $E(|\Psi\rangle) > E(|\Phi\rangle)$  for the von Neumann or any other single choice) [19], so that Eq. (33) warrants a rigorous deep entanglement increase with increasing  $N$  which is physically linked to the possibility of pure state conversion by LOCC to the lower  $N$  history.

We finally mention that in the continuous limit, the Renyi entropy of a gaussian distribution  $N(\mu, \sigma)$  is just

$$S_q^R(\sigma) = C_q + \log \sigma, \quad (38)$$

exhibiting them all the same dependence with the standard deviation  $\sigma$  except for a  $\sigma$ -independent constant  $C_q = \frac{1}{2}[\log(2\pi) + \frac{1}{q-1} \log q]$ . The result for the von Neumann entropy is recovered for  $q \rightarrow 1$  ( $\frac{1}{q-1} \log q \rightarrow \log e$ ). A similar result is valid for the Renyi entropy of the exponential distribution  $f(x) = \sigma^{-1}e^{-x/\sigma}$ ,  $x \geq 0$ , for which  $\langle x \rangle = \sigma = \sqrt{\langle x^2 \rangle - \langle x \rangle^2}$  and (38) holds with  $C_q = \frac{1}{q-1} \log q$ . We have used  $S_q^R(f) = \frac{1}{1-q} \log \int_{-\infty}^{\infty} f^q(x) dx$  when applied to a continuous distribution  $f(x)$ .

Thus, an approximate gaussian or exponential distribution of eigenvalues of  $\mathbf{O}$  will lead roughly to entanglement entropies  $E_q$  differing in a  $\sigma$ -independent constant for distinct  $q$ , and exhibiting a similar behavior with  $\sigma$ .

## E. Coherent states and overlap matrix

The well-known coherent states [50] represent a family of quantum harmonic oscillator states depending on a continuous variable, already introduced by E. Schrödinger [51] and later developed by R. Glauber in relation with the quantum theory of coherence and quantum optics [52], and also by E. Sudarshan [53]. These states possess minimum uncertainty,  $\Delta_Q \Delta_P = \hbar/2$ , and can then be said to be the “closest” ones to classical states. Starting from bosonic creation and annihilation operators  $a, a^\dagger$ ,  $[a, a^\dagger] = 1$ , with vacuum state  $|0\rangle$  ( $a|0\rangle = 0$ ), a coherent state  $|\alpha\rangle$  is defined as the unique (except for phase and normalization) eigenstate of the annihilation operator  $a$  with eigenvalue  $\alpha$ :

$$a|\alpha\rangle = \alpha|\alpha\rangle. \quad (39)$$

Such state exists  $\forall \alpha \in \mathbb{C}$  and is just a displaced vacuum,

$$|\alpha\rangle = D(\alpha)|0\rangle = e^{-\frac{|\alpha|^2}{2}} e^{\alpha a^\dagger} |0\rangle \quad (40a)$$

$$= e^{-\frac{|\alpha|^2}{2}} \sum_{n=0}^{\infty} \frac{\alpha^n}{\sqrt{n!}} |n\rangle, \quad (40b)$$

where  $D(\alpha) = e^{\alpha a^\dagger - \alpha^* a}$  is the unitary displacement operator ( $D^\dagger(\alpha) a D(\alpha) = a + \alpha$ ),  $|n\rangle = \frac{(a^\dagger)^n}{\sqrt{n!}} |0\rangle$  the Fock states ( $a^\dagger a |n\rangle = n |n\rangle$ ) and we used  $e^{\alpha a^\dagger + \beta a} = e^{\alpha\beta/2} e^{\alpha a^\dagger} e^{\beta a}$ . Thus, they lead to a Poisson distribution  $|\langle n|\alpha\rangle|^2 = \frac{|\alpha|^{2n}}{n!} e^{-|\alpha|^2}$  over the Fock states, with  $|\alpha|^2 = \langle a^\dagger a \rangle_\alpha$  the average boson number ( $\langle O \rangle_\alpha := \langle \alpha | O | \alpha \rangle$ ).

Besides, if  $q = \frac{a+a^\dagger}{\sqrt{2}}$ ,  $p = \frac{a-a^\dagger}{\sqrt{2}i}$  are the associated dimensionless coordinate and momentum ( $[q, p] = i\mathbb{1}$ ), we have  $\langle q \rangle_\alpha = \sqrt{2} \text{Re}(\alpha)$ ,  $\langle p \rangle_\alpha = \sqrt{2} \text{Im}(\alpha)$  and  $\langle q^2 \rangle_\alpha - \langle q \rangle_\alpha^2 = \langle p^2 \rangle_\alpha - \langle p \rangle_\alpha^2 = \frac{1}{2}$ , hence leading to minimum uncertainty  $\Delta q \Delta p = 1/2$ . In quantum optics they are the states which best describe a laser beam [50].

The coherent states fulfill the completeness relation  $\frac{1}{\pi} \int |\alpha\rangle \langle \alpha| d^2\alpha = \mathbb{1}$  and are nonorthogonal, having a gaussian overlap

$$\langle \alpha' | \alpha \rangle = e^{-\frac{1}{2}(|\alpha|^2 + |\alpha'|^2 - 2\alpha\alpha'^*)}. \quad (41)$$

In particular, for  $\alpha, \alpha'$  real, this overlap takes the form

$$\langle \alpha' | \alpha \rangle = e^{-\frac{1}{2}(\alpha - \alpha')^2}, \quad (42)$$

corresponding to real gaussian wave functions  $\langle q|\alpha\rangle = \frac{1}{\sqrt{\pi}} e^{-(q - \sqrt{2}\alpha)^2/2}$  ( $\langle \alpha' | \alpha \rangle = \int_{-\infty}^{\infty} \langle \alpha' | q \rangle \langle q | \alpha \rangle dq$ ).

Eq. (42) will be here of most importance. In first place it shows that any matrix with gaussian elements  $M_{\alpha\alpha'}^{(2)} = e^{-\frac{1}{2}(\alpha - \alpha')^2}$  is positive semidefinite for any set of real numbers  $\alpha, \alpha'$ , since it represents an overlap matrix of coherent states, i.e., a Gram matrix (a matrix of inner products). These matrices are hermitian and positive semidefinite, and singular only if the states involved are linearly dependent, their rank (number of nonzero eigenvalues) indicating the number of linearly independent states generated by the set considered. As any finite set of distinct coherent states is linearly independent, the ensuing overlap matrix will have full rank unless some of the  $\alpha$ 's are coincident.

It is worth noticing that the exponent 2 in the overlap function is the highest exponent yielding a positive semidefinite matrix. In general, a matrix of elements

$$M_{\alpha\alpha'}^{(p)} = e^{-|\alpha - \alpha'|^p/2} \quad (43)$$

is not necessarily positive semidefinite for  $p > 2$ , as can be checked numerically.

The gaussian case  $M_{\alpha\alpha'}^{(2)}$ , then lies at the “border” of the admissibility region for positivity. Its positivity can be explicitly verified from the Fourier identity  $e^{-\alpha^2/2} = \frac{1}{\sqrt{2\pi}} \int_{-\infty}^{\infty} e^{i\alpha t} e^{-t^2/2} dt$ , valid  $\forall \alpha \in \mathbb{R}$ . Hence  $\mathbf{v}^\dagger M^{(2)} \mathbf{v} =$

$\sum_{\alpha, \alpha'} v_{\alpha'}^* v_{\alpha} M_{\alpha' \alpha}^{(2)} = \frac{1}{\sqrt{2\pi}} \int_{-\infty}^{\infty} |v(t)|^2 e^{-t^2/2} dt \geq 0 \forall$  vector  $\mathbf{v}$  of arbitrary elements  $v_{\alpha} \in \mathbb{C}$ , with  $v(t) = \sum_{\alpha} e^{i\alpha t} v_{\alpha}$ . This integral vanishes only if  $v(t) = 0 \forall t$ , entailing  $\mathbf{v} = \mathbf{0}$  for any finite set of distinct real numbers  $\alpha$ .

Finally, a history of coherent states  $|\alpha_n\rangle$ ,  $n = 0, \dots, N-1$ , can be generated as in Eq. (7), using (40a):

$$|\Psi\rangle = \frac{1}{\sqrt{N}} \sum_n |\alpha_n\rangle \otimes |n\rangle \quad (44a)$$

$$= \frac{1}{\sqrt{N}} \left( \sum_n D(\alpha_n) \otimes |n\rangle \langle n| \right) (|0\rangle \otimes |\bar{0}\rangle), \quad (44b)$$

where  $|0\rangle$  denotes the vacuum state of the boson and  $|\bar{0}\rangle = \frac{1}{\sqrt{N}} \sum_n |n\rangle = H_N |n=0\rangle$ .

### F. History state formalism for time series

In this section we present the application of the history state formalism to time series. In order to define the history state for a time series of real numbers  $p_n$ ,  $n = 0, \dots, N-1$ , we assign to each  $p_n$  a coherent state  $|\alpha_n\rangle$  of the form (40b), namely

$$|\alpha_n\rangle = |p_n/\sigma\rangle, \quad (45)$$

where  $\sigma \in \mathbb{R}$  is a scale fixing the threshold of distinguishability between two different values of the  $p_n$ 's. This scale will remain fixed for all  $p_n$  of a given history. The ensuing history state is then given by Eq. (44).

Since  $p_n \in \mathbb{R}$ , the overlap between the associated coherent states becomes, using Eq. (42),

$$\langle \alpha_n | \alpha_m \rangle = e^{-(p_n - p_m)^2 / (2\sigma^2)}. \quad (46)$$

Hence  $\langle \alpha_n | \alpha_m \rangle \approx 0$  if  $|p_n - p_m| \gg \sigma$  while  $\langle \alpha_n | \alpha_m \rangle \approx 1$  if  $|p_n - p_m| \ll \sigma$ . Different choices of  $\sigma$  will provide more or less sensitivity to fluctuations in the values of the  $p_n$ 's: a small  $\sigma$  will narrow the gaussians, such that most states will be counted as distinct, leading to a larger entanglement entropy of the history state, whereas a large  $\sigma$  will widen the gaussians, hence counting many states as similar and yielding a smaller entropy. A standard criterion is to choose  $\sigma$  of the order of some percentage of the range of values involved, so that a difference  $|p_n - p_m| \approx \sigma$  in (46) leads to an overlap  $\langle \alpha_i | \alpha_j \rangle \approx 0.6$ , i.e., a  $\approx 40\%$  drop in comparison with its maximum, indicating that the associated values start to be distinguishable.

While in the von Neumann case we need the eigenvalues of this overlap matrix for computing the entanglement entropy exactly, the quadratic Renyi entropy of Eqs. (29)–(30) can be directly evaluated:

$$E_2(S, T) = -\log \left( \frac{1}{N^2} \sum_{n, m} |\langle \alpha_n | \alpha_m \rangle|^2 \right) \quad (47)$$

$$\approx \log N - \frac{2}{N} \sum_{n < m} e^{-\frac{(p_n - p_m)^2}{2\sigma^2}}, \quad \sigma \ll \Delta_{\min} \quad (48)$$

where (48) is the approximation for small overlaps or equivalently small  $\sigma$ , such that  $\sum_{m < n} |\langle \alpha_n | \alpha_m \rangle|^2 \ll N$ , i.e. almost orthogonal states ( $\Delta_{\min}$  denotes the minimum absolute difference).

On the other hand, if the aim is to measure just significant variations, one could choose a sufficiently large  $\sigma$  such that  $(p_n - p_m)^2 / \sigma^2 \ll 1$  and hence,

$$\langle \alpha_n | \alpha_m \rangle \approx 1 - \frac{(p_n - p_m)^2}{2\sigma^2}. \quad (49)$$

In this limit, opposite to that of (48), Eq. (47) becomes

$$E_2(S, T) \approx -\log \left( 1 - \frac{2}{N^2 \sigma^2} \sum_{n < m} (p_n - p_m)^2 \right) \quad (50a)$$

$$\approx \frac{2}{N^2 \sigma^2} \sum_{n < m} (p_n - p_m)^2 \quad (50b)$$

$$= \frac{2}{\sigma^2} \left[ \frac{1}{N} \sum_n p_n^2 - \left( \frac{1}{N} \sum_n p_n \right)^2 \right], \quad \sigma \gg \Delta_{\max} \quad (50c)$$

which is just proportional to the *fluctuation*, i.e. the variance of the  $p_n$ 's in the history considered ( $\Delta_{\max}$  is the maximum price difference). Moreover, for  $p_n > 0 \forall n$ , one could also use the *logarithm* of the values  $p_n$  in order to measure just very significant variations, i.e.,  $p_n \rightarrow \log p_n$  in Eqs. (45) and (49)–(50).

## III. APPLICATION TO FINANCIAL TIME SERIES

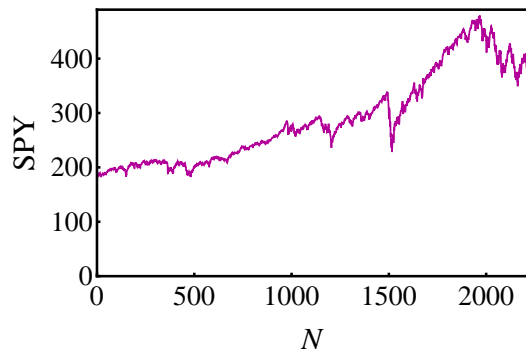


FIG. 1. Opening values of the SPY (in USD) as a function of the elapsed number of days  $N$  along the period 17 March 2014 – 30 December 2022 [54].

### A. Full history analysis

We now apply this formalism to the analysis of the evolution of financial time series. We first consider the SPY, the code for the ETF which tracks the SPX stock market index, in the period from March 17 2014 to December 30 2022, comprising 2206 trading days. We employ the daily opening price  $p_n$  as the representative price of that day. They are shown in Fig. 1 with data taken from [54].

We first consider the history state associated to previous prices for  $N$  contiguous trading days, starting at March 17 2014, for  $1 \leq N \leq 2206$ . We use the coherent state embedding (45).

### 1. Entanglement entropy

We depict in Fig. 2 the entanglement entropy of the history state up to day  $N$  for the whole period, for different values of  $\sigma$  in (45)–(46). We have set  $\sigma = \sigma_r \sigma_0$ , with  $\sigma_0 = 1$  USD taken as unit and  $\sigma_r$  a relative dimensionless width. We show results for the two entropic measures that will be employed in what follows: the von Neumann entropy (8)–(16), denoted as  $E_1$  in the plots, and the quadratic Renyi entropy (30), denoted as  $E_2$ .

Both entanglement entropies, which measure essentially the logarithm of the effective number of distinct prices visited in the history, evolve similarly except for an almost constant vertical shift  $\Delta E \approx 0.5$ , for each fixed value of  $\sigma_r$ , though  $E_1$  exhibits a slightly higher sensitivity. They both display a rather smooth steady increase for increasing  $N$  if  $N \gtrsim N_c \approx 585$ , reflecting the upward trend of prices, as new values are “visited”. Nonetheless, they also show some small slope discontinuities at certain days, with short intervals of negative slope for  $N < N_c$ , which indicate essentially that no distinct states (i.e. prices) are visited at those days.

Remarkably, the behavior for distinct widths  $\sigma_r$  is also similar in the indicated range, except for an almost constant difference which depends on the ratio of the  $\sigma_r$ : The entanglement entropy of the history obviously increases for decreasing  $\sigma_r$ , i.e., increased resolution. Roughly,  $E_{\sigma_r=0.5} - E_{\sigma_r=1} \approx 0.9$  for  $N \gtrsim 300$ , while  $E_{\sigma_r=1} - E_{\sigma_r=10} \approx 3.1$ , in agreement with a dependence similar to Eq. (38). We also show for comparison the common maximum entropy  $E_{\max} = \log N \forall q > 0$  that can be obtained up to that day, which corresponds essentially to the  $\sigma_r \rightarrow 0$  limit and would be reached only if a new distinct state, i.e., a well distinguishable asset price not contained in previous history, were reached at each day. For the chosen values of  $\sigma_r$ ,  $E_{\max}$  is much higher than the actual history entropies, indicating a price behavior well detached from the saturation limit.

In the bottom panel we show the effective number (17) of distinct states  $|\alpha_n\rangle$  visited during the evolution, for the von Neumann and quadratic Renyi entropies. It is verified that  $N_E$  lies well below  $N$ . The behavior for both entropies is again quite similar, since their ratio for fixed  $\sigma_r$  and distinct entropy, as well as for fixed entropy and distinct  $\sigma_r$ , is almost constant due to the roughly constant entropy difference shown in the upper panel. Again,  $N_E$  shows a slightly higher sensitivity in the von Neumann case. The slope variations, indicative of changes in the price evolution regime, and the intervals of entropy decrease, are more clearly appreciable.

### 2. Entanglement spectrum and majorization

In order to obtain a deeper picture of the entanglement entropy evolution, we now analyze the entanglement spectrum of the history state and the associated majorization properties.

In the top panel of Fig. 3, we show the evolution of the von Neumann entanglement entropy  $E = E_1$  (10) for

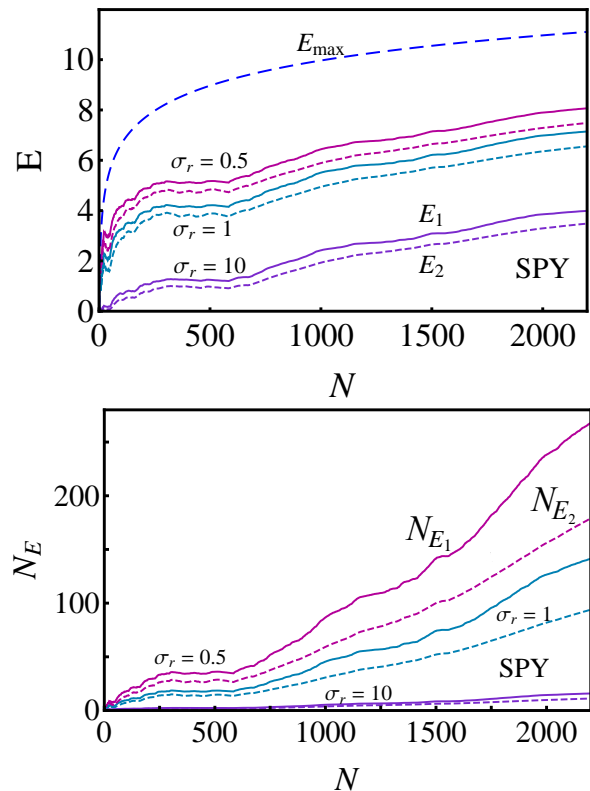


FIG. 2. Top panel: The von Neumann (solid lines) and quadratic Renyi (short dashed lines) entanglement entropies  $E_1$  and  $E_2$  respectively, Eqs. (16)–(30), of the history state associated to the SPY prices for the first  $N$  days,  $1 \leq N \leq 2206$ , starting at March 2014, for distinct values of the relative width  $\sigma_r$ . For reference the maximum attainable value  $E_{\max} = \log_2 N$  (the same for both entropies, representing the  $\sigma_r \rightarrow 0$  limit), is also depicted. Bottom: The corresponding effective number of distinct states visited in the same period, Eq. (17), for the indicated entropies, as a function of  $N$ .

$\sigma_r = 1$ , together with the corresponding partial sums

$$\Sigma_\ell^{(N)} = \sum_{k=1}^{\ell} \lambda_k^{(N)} \quad (51)$$

of the eigenvalues  $\lambda_k^{(N)}$  of the normalized overlap matrix for the first  $N$  steps, which determine their majorization properties (section IID and App. A). It is seen that it is possible to clearly identify two different regimes during the evolution. For  $N \gtrsim N_c = 585$  (vertical dashed line) all partial sums (51) after  $N$  steps decrease with increasing  $N$ , entailing that majorization relations (34)–(35) are fulfilled and hence the universal entropy increase regime I is taking place, i.e., not only the depicted von Neumann entropy, but all entanglement entropies, are increasing. This behavior indicates essentially that “new” prices are incorporated to the evolution at each step.

In contrast, in the previous sector  $N \lesssim N_c$  there are values or even intervals of  $N$  for which the partial sums are not majorized by those of previous  $N$  and this is

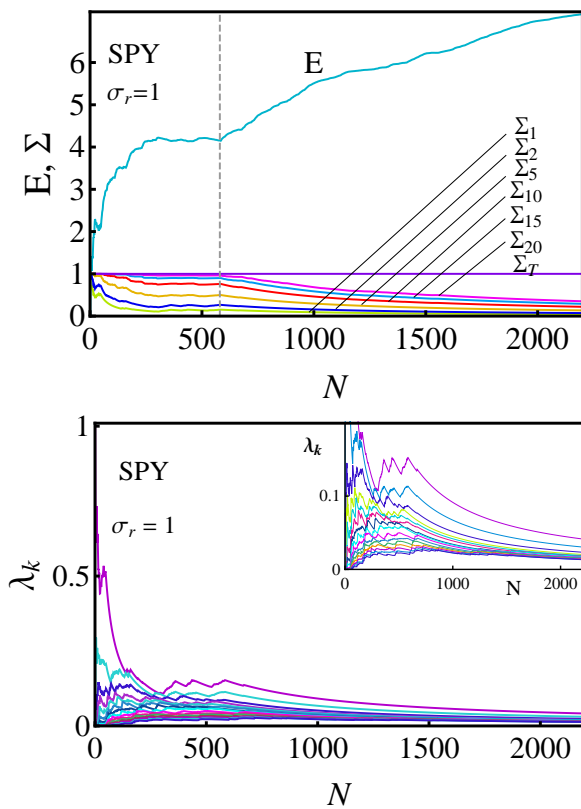


FIG. 3. Top panel: The entanglement entropy  $E = E_1$  of the history state as a function of the number of elapsed days  $N$  for  $\sigma_r = 1$  in the whole period, and the associated partial sums  $\Sigma_\ell = \sum_{k=1}^{\ell} \lambda_k$  of the eigenvalues of the overlap matrix, as a function of  $N$ , for the indicated values of  $\ell$ , with  $\Sigma_T = 1$  the total sum. The vertical dashed line signals a regime change after which all partial sums tend to decrease, indicating majorization for increasing  $N$  after this point. Bottom panel: The corresponding entanglement spectrum of the history state as a function of the number of elapsed days  $N$ . We depict the first 15 eigenvalues  $\lambda_k$  of the overlap matrix  $\mathbf{O}_N$ , (which are those of  $\rho_S$  and  $\rho_T$ ), with the elements (46). The inset shows in more detail the behavior of the lowest eigenvalues.

reflected in the rather stable value of the entanglement entropy for  $\frac{1}{2}N_c \lesssim N \lesssim N_c$ , above the initial increase. In this intermediate region no strict majorization relation takes place between the spectra for different  $N$  (type III regime). Besides, at certain values of  $N$  the partial sums are approximately majorized by those of the next step, leading to an almost universal slight entropy decrease at these points (type II regime). The vertical line at  $N = N_c$  then signals a noticeable change in the behavior of the partial sums and the associated entropy, which enables to identify different regimes.

In the bottom panel of Fig. 3 we show the evolution with  $N$  of the entanglement spectrum of the normalized overlap matrix  $\mathbf{O}_N$  of Eq. (11), with the elements (46). It seen that in the sector  $N \gtrsim N_c$  the largest eigenvalues exhibit a rather continuous decrease with increasing

$N$ , reflecting the incorporation of new small eigenvalues, i.e., orthogonal states in the history, in agreement with the universal entropy increase regime I. There is here a progressive increment in the number of small eigenvalues whose magnitudes initially increase. In contrast, in the sector  $N \lesssim N_c$  above the initial increase, the eigenvalues exhibit noticeable oscillations (see also inset), leading to a different regime in the partial sums (type III, no strict majorization) and entropy, except for short intervals of almost type II behavior.

## B. Evolution of monthly histories

It is also possible to use the formalism for other types of analyses of the time series along a given period, by considering partial histories, i.e., histories along a fixed shorter time interval. In this way the ensuing entanglement entropy will be a measure of the effective number of distinct prices reached in such interval, providing an indicator of the volatility of the asset in the latter. The evolution of such entropies within the total period will then provide a picture of the volatility variation.

In this section we consider the evolution of the SPY asset along a period of one month, corresponding to at most 21 trading days. Accordingly, we construct the history state for each month and evaluate the associated entanglement entropy and spectrum. We then examine these quantities for a total period of 120 months, from March 19 2014 to March 15 2024 (120 trading months).

In the top panel of Fig. 4 we show results for the von Neumann entanglement entropy  $E = E_1$  of the history of each month together with the corresponding partial sums of the eigenvalues of the normalized overlap matrix  $\mathbf{O}_{N_m}$  ( $N_m \leq 21$ ) for the sequence of 120 months of the period of Figs. 2 and 3 with  $\sigma_r = 1$ . The vertical dashed line at month 73 indicates that at this month all partial sums are lower than those of any other month in the whole period, implying that the spectrum of this month is majorized by that of any other month. This entails a maximum monthly entanglement entropy at this month, for *any* choice of entropy (and not just for the depicted von Neumann case), indicating the month with a maximum number of distinct asset prices for the  $\sigma$  considered, i.e., of maximum volatility. On the other hand, the vertical dashed line at month 40 indicates the month of minimum entropy, where the partial sums are all greater than those of any other month and hence the spectrum majorizes that of any other month. Hence, it indicates the month of minimum price dispersion, i.e., minimum volatility.

In the bottom panel of Fig. 4, we show the evolution of the 10 largest eigenvalues of the monthly history entanglement spectrum, along the whole period. Maximum (minimum) entropy corresponds obviously to minimum (maximum) dispersion of eigenvalues. From the associated Schmidt decomposition, we can say that these eigenvalues represent the normalized probability distribution

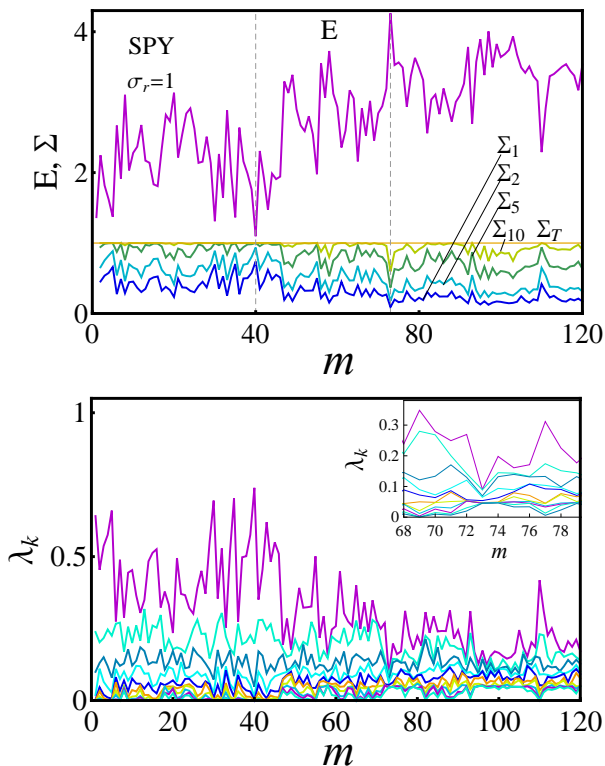


FIG. 4. Top: The entanglement entropy  $E = E_1$  of the one-month history state for 120 months  $m$  starting at March 17 2014, for  $\sigma_r = 1$ , together with the associated partial sums  $\Sigma_\ell = \sum_{i=1}^{\ell} \lambda_k$  of the entanglement spectrum for each month for  $\ell = 1, 2, 5, 10$ . The vertical dashed lines indicate months 73 and 40, where the monthly entropy reaches its maximum and minimum respectively, and accordingly, the monthly partial sums have their minimum and maximum. Bottom: The corresponding entanglement spectrum of the monthly history in the same period. We depict the first 10 eigenvalues  $\lambda_k$  of the normalized overlap matrix for each month. The inset shows in more detail the behavior of the lowest eigenvalues around the region of highest monthly volatility ( $68 \lesssim m \lesssim 79$ ).

of the actual distinct prices (according to the chosen  $\sigma_r$ ) in the corresponding month. The inset depicts the detailed behavior of the main eigenvalues in the vicinity of the month of maximum entropy (i.e., maximum volatility). At the maximum they tend to be almost degenerate, having minimum dispersion.

In Fig. 5, we show the evolution of the corresponding effective number (17) of monthly visited “states”  $N_E$  for the von Neumann entanglement entropy, and compare it with the monthly VIX index values in the same period, taken from [55]. There is clearly a good qualitative agreement between both quantities, with the maxima of  $N_E$  matching those of the VIX. Accordingly, the maximum of the monthly values of  $N_E$  signals the largest peak of the monthly VIX values, located at month 73. Also, the minimum  $N_E$ , at month 40, lies close to the minimum of the VIX. Hence,  $N_E$  can be considered as an alternative measure of volatility.

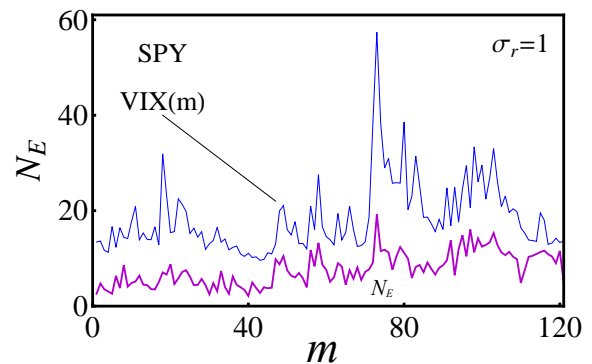


FIG. 5. Number of effective visited states  $N_E$  for each month, in the same case of Fig. 4. The monthly VIX values for the same period are also depicted. There is a close qualitative agreement between both quantities.

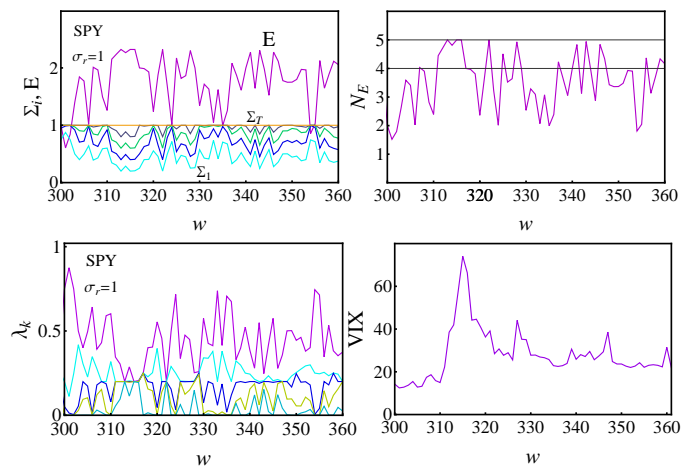


FIG. 6. Top left: The von Neumann entanglement entropy  $E = E_1$  of one week history state for the indicated 60 weeks period together with the associated partial sums  $\Sigma_\ell$ , (only  $\ell = 1$ , and  $\ell = 5 = T$  are indicated) of the entanglement spectrum for each week. The VIX experiences a noticeable variation (bottom right panel) for the weeks with highest occupation (top right panel) and highest degeneracy (bottom left panel). Top right: Behavior of the effective number of visited states  $N_E$  (17) in the same period. It is seen that  $N_E$  takes its maximum value  $N_E = 5$  for the weeks for which there is full degeneracy in the spectrum (see text). Bottom left: Evolution of the entanglement spectrum for the same period. It is seen that the spectrum exhibits total or partial degeneracy, which may indicate different degrees of change in the volatility of the asset (see text). Bottom right: Behavior of the VIX index in the same period.

### C. Evolution of weekly histories

In order to examine in detail the behavior around a specific point, in this section we study the SPY histories for just one week, comprising at most 5 consecutive trading days, and analyze their evolution in a surrounding interval. We will focus on the interval comprising the max-

imum weekly volatility, which corresponds essentially to the months of maximum monthly volatility, where the VIX index experiences its largest variation. Namely an interval of 60 weeks from week 300 up to week 360 in the whole previous period of 522 weeks from March 17 2014 to March 15 2024.

In the top left panel of Fig. 6 we show the evolution of the weekly von Neumann entanglement entropy  $E = E_1$  in this interval, together with the corresponding partial sums  $\Sigma_\ell$  for  $\ell = 1, \dots, 5$  ( $N_w \leq 5$ ). At weeks 313 and 315, the partial sums are minimum, i.e., lower than those of any other week, and accordingly, the entropy is maximum, reaching saturation,  $E = \log N_w$ , indicating a plain uniform distribution. Majorization occurs and any entropy will then be maximum at these two weeks.

The top right panel shows the effective number of visited states  $N_E$  (17) in the corresponding week. It obviously saturates at the weeks of maximum entropy, signalling maximum weekly volatility. On the left bottom panel we show the detailed evolution of the set of eigenvalues (entanglement spectrum) of  $\mathbf{O}_{N_w}$  for each week along the same period. The presence of complete or almost complete degeneracy in the spectrum can be clearly identified at weeks 313, 315, and some other values (like 322, 329, etc.), which coincide with the highest maxima of  $N_E$  ( $N_E > 4$ ) of the top right panel, hence indicating high volatility. In fact, weeks for which the spectrum is fully or partially degenerate correspond approximately to those weeks where maxima or abrupt changes in the VIX values (bottom right panel) occur. This weekly analysis enables then to rapidly recognize periods of high volatility in the asset.

#### D. Weekly and monthly logarithmic histories

In order to explore other approaches feasible within the history state based formalism, and with the aim of obtaining an improved resolution of the most prominent fluctuations above the baseline noise, in this section we analyze the histories of the *logarithm* of the prices. In this case we set  $\alpha_n = \log[p_n/p_0]/\sigma$  in the quantum coherent state representation, where  $p_0$  is some price scale. Then, according to Eq. (42), their overlaps become  $\langle \alpha_n | \alpha_m \rangle = e^{-\log^2[p_n/p_m]/(2\sigma^2)}$ , obviously  $p_0$  independent and determined just by the logarithm of the prices ratios.

Since such logarithms are relatively small, this approach will essentially pick up the largest price variations. Moreover, already for not too small values of  $\sigma$  (i.e.  $\sigma \gtrsim 1$ ), we are already in the large overlap regime of Eq. (49), such that the  $q = 2$  Renyi entanglement entropy of the associated history state approaches Eqs. (50). It then becomes proportional to  $\sigma^{-2}$  times the *fluctuation* of the logarithm of the asset price along the  $N$ -step history, according to Eq. (50c), and hence to  $\frac{1}{N^2} \sum_{m < n} \log^2(p_n/p_m)$

according to (50b), leading to

$$E_{2_{\log}} \approx \frac{2}{N^2 \sigma^2} \sum_{n < m} \log^2(p_n/p_m). \quad (52)$$

In the following we then employ the quadratic Renyi entropy with  $\sigma = 1$ , such that its value is essentially the logarithmic fluctuation of the prices, Eq. (52), except for a scale factor  $\propto \sigma^{-2}$ .

##### 1. SPY Histories

We first apply previous scheme to further analyze the evolution of the SPY along the whole previous period of ten years, based on the variation of weekly and monthly logarithmic history entropies (Eq. (52)). For reference we compare results with those of the corresponding VIX for the SPY.

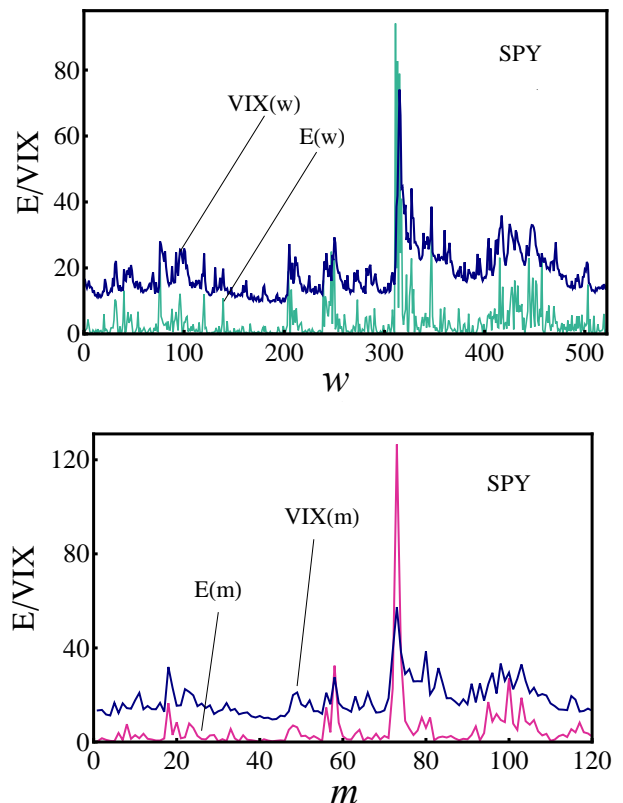


FIG. 7. Weekly (top) and monthly (bottom) evolution of the quadratic Renyi history entanglement entropy, employing the logarithm of SPY prices (see text), together with the corresponding reference VIX values for SPY along the whole previous period.

It is worth mentioning that the VIX needs the input of several options prices in a range of around 30 days, and can be cumbersome to calculate for a type of asset different from the SPY. Here we examine the ability of the previous logarithmic entropic measure of volatility to account for the main features of VIX index evolution.

In Fig. 7 we depict the evolution of the VIX index for a period of ten years as a function of time in weeks (top panel) and months (bottom panel). In both cases, we have compared the VIX index with the entropic measure of volatility given by the  $E_2^R$  entropy (30) using the logarithm of prices, which leads essentially to Eq. (52). In the top panel we show weekly results for a period of 522 weeks, while in the bottom panel the monthly results for a period of 120 months. For a better visualization and comparison with the VIX index in the same plot, we have scaled our results by multiplying them by a fixed factor (equivalent to a given  $\sigma$  in the approximation (52)).

It is seen that our measure tends to reproduce the sudden changes observed in the VIX measure, with the peaks of the entropic measure matching the most relevant changes in the VIX evolution. It is also able to distinguish the main peaks which reflect large volatility in the asset, for both weekly and monthly evolutions. The use of the logarithm tends to filter the noise, providing an improved signal-to-noise ratio, being more sensitive to the higher price fluctuations.

## 2. Results for Gold and Bitcoin

Finally, we also include results for GLD [56] and BTC [57], where comparisons between the present entropic measure of volatility and the standard volatility measures for these assets (CBOE Gold ETF Volatility Index for GLD [58] and CVI for BTC [59]) are shown for the same previous period of 10 years in the case of gold, and a 298 weeks period for BTC, from March 31 2019 to 20 December 2024.

In Fig. 8 we depict the evolution of the VIX index for GLD for a period of ten years as a function of weeks (top panel) and months (bottom panel). In the top panel, the results correspond to a period of 535 weeks, where the overlaps were evaluated for periods of one week (5 days), whereas in the bottom panel, results are for the same interval corresponding to 120 months, whereas the overlaps were evaluated for periods of one month (21 days). In both cases, we have employed the entropic measure of volatility given by the  $q = 2$  Renyi history entanglement entropy (50c), employing the logarithm of the GLD prices. We have also employed a convenient scale in order to compare our results with those of the VIX index.

In Fig. 9 we show the evolution of the CVI index for BTC, together with the evolution of our entropic measure of volatility as a function of time in weeks. The entropic measure was evaluated with the  $E_2^R$  entropy, and we have employed again the logarithm of the BTC prices. We have analyzed a period corresponding to 298 weeks, starting in March 31 2019.

As in the case of the SPY, results for these two different assets show that the entropic measure of volatility is able to clearly identify those weeks or months which are characterized by a large volatility of the asset. There is a good agreement between results from our approach

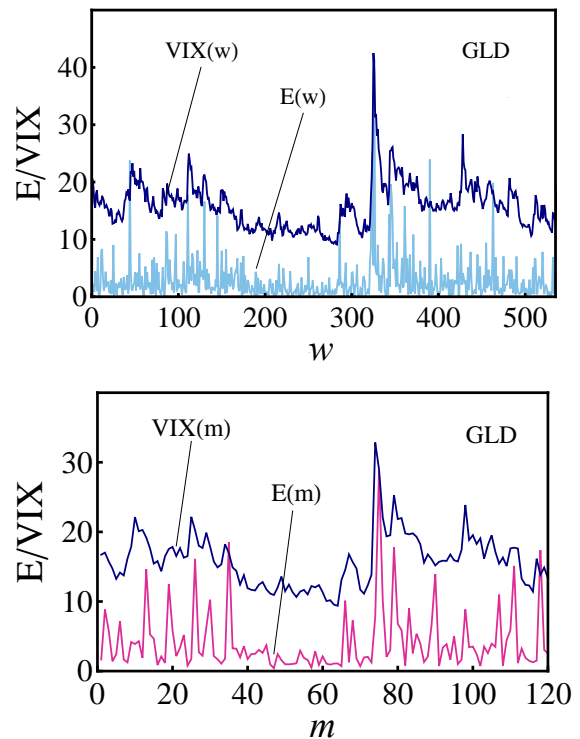


FIG. 8. Top: Weekly evolution of the quadratic Renyi history entanglement entropy, employing the logarithm of Gold prices, (50c), together with the corresponding reference VIX values along a period of 535 weeks. Bottom: Monthly evolution of the same quantities for a period of 120 months.

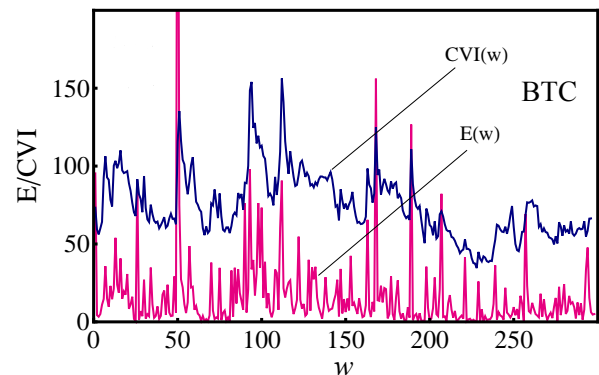


FIG. 9. Weekly evolution of the quadratic Renyi history entanglement entropy, employing the logarithm of BTC prices, and the reference CVI values for BTC, along a 298 weeks period (see text).

and those of the standard measures of volatility corresponding to the evolution of each asset. We see that in general, for the analyzed assets, our entropic measure has a better signal-to-noise ratio than the standard volatility indicators when using the logarithm of prices, as peaks are more prominent than the baseline volatility as compared to the VIX and the CVI.

#### IV. CONCLUSIONS

We have introduced a general method for analyzing time series from the new perspective provided by the quantum history state formalism. This framework leads to the concept of system-time entanglement, which constitutes a measure of the effective number of orthogonal (i.e., fully distinguishable) states visited during the whole evolution considered. It is fully determined by the eigenvalues of the overlap matrix of the evolved states, which here form the entanglement spectrum. It also emerges as mutual information of the decohered mixed history state.

The history state associated to a given time series is then defined through a scaled quantum coherent state embedding of the time series data. Through the corresponding gaussian overlaps between these states, a consistent smooth transition between coincident and clearly distinguishable data is achieved. The associated entanglement entropy then provides a measure of the effective number of distinct data in the series, relative to the reference width. The ensuing entanglement spectrum represents the relative frequency of appearance of the effective “orthogonal” states of the evolution, the latter emerging from the Schmidt decomposition of the history state. In addition, a rigorous analysis of the entanglement spectrum based on majorization theory allows one to identify distinct evolution regimes, including those characterized by a universal entanglement entropy increase or decrease.

The formalism was applied to examine financial time series, starting with the price evolution of the SPY asset. Through different types of histories, including the evolution of the SPY along a full history in III A, a monthly history in III B, and a weekly history in III C, it was seen that the entanglement entropy, the associated effective number of visited states  $N_E$ , and the entanglement spectrum, provide reliable indicators of relevant properties of the series. In particular, from the majorization properties of the entanglement spectrum, different evolution regimes in the full history of the SPY could be identified, whereas through monthly and weekly histories, a good correspondence between the entanglement entropy (or the ensuing  $N_E$ ) with the pertinent VIX index was achieved, thus detecting periods of high volatility.

In order to obtain an improved visualization of main variations, in III D we also explored weekly and monthly logarithmic histories and entanglement entropies, for SPY as well as for GLD and BTC, and compared them with the corresponding volatility measures. A close qualitative agreement between them was obtained, as highlighted from the matching in the position of the peaks observed in the figures. Moreover, the quadratic Renyi entropy of the logarithmic history was shown to be closely related to the logarithmic fluctuation.

In summary, the present quantum-based formalism is able to provide deep insights into the complex behavior of time series, including quantities showing a good agreement with standard volatility indicators of financial series. The associated entanglement spectrum, an essential

quantum concept, can also provide useful information for identifying different regimes. This quantum formulation also opens the way to other possibilities, from quantum simulation of the full history to the implementation of quantum computation protocols for time averages, which are currently under investigation.

#### ACKNOWLEDGMENTS

Authors acknowledge support from CONICET (F.L., N.C., A.B) and CIC (R.R.) of Argentina. Work supported by CONICET PIP Grant No. 11220200101877CO.

#### Appendix A: Majorization and mixedness.

Let  $\mathbf{p} = (p_1, p_2, \dots, p_n)$  and  $\mathbf{q} = (q_1, q_2, \dots, q_n)$  be two probability distributions ( $p_i \geq 0$ ,  $\sum_i p_i = 1$  and similarly for  $\mathbf{q}$ ). If we sort the components of  $\mathbf{p}$  and  $\mathbf{q}$  in decreasing order, such that  $p_1 \geq p_2 \geq \dots \geq p_n$ ,  $q_1 \geq q_2 \geq \dots \geq q_n$ , it is said that  $\mathbf{q}$  is *majorized* by  $\mathbf{p}$  [18] or, in symbols,

$$\mathbf{q} \prec \mathbf{p}, \quad (\text{A1})$$

iff the following inequalities are all fulfilled:

$$\sum_{j=1}^i q_j \leq \sum_{j=1}^i p_j \quad \forall i = 1, \dots, n-1, \quad (\text{A2})$$

with equality for  $i = n$ . Thus, if  $p_i = \delta_{ik}$  for a certain  $k$  (maximum certainty)  $\Rightarrow \mathbf{q} \prec \mathbf{p}$  for any distribution  $\mathbf{q}$ , whereas for a uniform distribution  $q_i = 1/n \forall i$  (maximum uncertainty or mixedness) we have  $\mathbf{q} \prec \mathbf{p}$  for any distribution  $\mathbf{p}$ . The concept of majorization also applies to probability distributions  $\mathbf{p} = (p_1, \dots, p_n)$  and  $\mathbf{q} = (q_1, \dots, q_m)$  with  $m \neq n$ , after padding with zeros that with the lesser number of elements.

If there exists a set of permutation matrices  $\{\Pi_i\}$  with probabilities  $r_i \geq 0$ ,  $\sum_i r_i = 1$  such that  $\mathbf{q} = \sum_i r_i \Pi_i \mathbf{p}$ , i.e. if  $\mathbf{q}$  is a convex combination of permutations  $\Pi_i$  of  $\mathbf{p}$ , then  $\mathbf{q} \prec \mathbf{p}$  and viceversa [18]:

$$\mathbf{q} \prec \mathbf{p} \iff \mathbf{q} = \sum_i r_i \Pi_i \mathbf{p}, \quad (\text{A3})$$

or, equivalently,

$$\mathbf{q} \prec \mathbf{p} \iff \mathbf{q} = D\mathbf{p}, \quad (\text{A4})$$

where  $D$  is a doubly stochastic matrix [18]. For this reason, if  $\mathbf{q} \prec \mathbf{p}$ , it is also said that the distribution  $\mathbf{q}$  is “more mixed” than  $\mathbf{p}$ .

Of course, given two distributions  $\mathbf{p}$ ,  $\mathbf{q}$ , it may occur that  $\mathbf{q} \not\prec \mathbf{p}$  and  $\mathbf{p} \not\prec \mathbf{q}$ , that is, neither  $\mathbf{p}$  or  $\mathbf{q}$  majorizes the other, entailing that majorization constitutes a partial order relation between probability distributions.

It can also be shown [18] that if  $\mathbf{q} \prec \mathbf{p}$  then  $\mathbf{q}$  has a larger entropy than  $\mathbf{p}$

$$\mathbf{q} \prec \mathbf{p} \Rightarrow S(\mathbf{q}) \geq S(\mathbf{p}). \quad (\text{A5})$$

where  $S(\mathbf{p}) = -\sum_i p_i \log p_i$  is the Shannon entropy. The converse relation obviously does not hold in general, i.e.,  $S(\mathbf{q}) \geq S(\mathbf{p}) \not\Rightarrow \mathbf{q} \prec \mathbf{p}$ , entailing that the concept of disorder provided by majorization is more stringent than that implied by the Shannon entropy.

On the other hand, if  $F$  is be the set of smooth concave functions  $f: [0, 1] \rightarrow \mathbb{R}$  that satisfy  $f(0) = f(1) = 0$ , it can be shown that [49]

$$\mathbf{q} \prec \mathbf{p} \iff \sum_i f(q_i) \geq \sum_i f(p_i) \quad \forall f \in F. \quad (\text{A6})$$

Recall that concavity means  $f[\alpha_1 p_1 + \alpha_2 p_2] \geq \alpha_1 f(p_1) + \alpha_2 f(p_2) \quad \forall \alpha_1, \alpha_2 \in [0, 1]$  with  $\alpha_1 + \alpha_2 = 1$ , with equality valid iff  $p_1 = p_2$  or  $\alpha_1 \alpha_2 = 0$ . For smooth  $f$ , concavity is equivalent to decreasing  $f'(p)$  for  $p \in (0, 1)$ .

For  $f \in F$ , the function [48, 49, 60, 61]

$$S_f(\mathbf{p}) = \sum_i f(p_i) \quad (\text{A7})$$

is a measure of the degree of ‘‘mixedness’’ associated with the probability distribution  $\mathbf{p}$ , and can be denoted as a *generalized trace form entropy*. It satisfies  $S_f(\mathbf{p}) \geq 0$  with  $S_f(\mathbf{p}) = 0$  only if  $p_i = \delta_{ij}$  for a certain  $j = 1, \dots, n$  (maximum certainty, while  $S_f(\mathbf{p})$  is maximum for  $p_i = 1/n \quad \forall i$  (maximum uncertainty). Furthermore, equation (A6) can be written as [49]

$$\mathbf{q} \prec \mathbf{p} \iff S_f(\mathbf{q}) \geq S_f(\mathbf{p}) \quad \forall f \in F. \quad (\text{A8})$$

Thus, if  $\mathbf{q} \prec \mathbf{p}$  then  $S_f(\mathbf{q}) \geq S_f(\mathbf{p}) \quad \forall S_f$ , and conversely, if  $S_f(\mathbf{q}) \geq S_f(\mathbf{p}) \quad \forall S_f$  then  $\mathbf{q} \prec \mathbf{p}$ . That is, they are sufficient to ensure the majorization relation. On the other hand, obviously  $S_f(\mathbf{q}) > S_f(\mathbf{p})$  for a given  $f$  does not necessarily imply  $\mathbf{q} \prec \mathbf{p}$ . The majorization relation cannot be captured by a single entropy, and is therefore stricter than the ‘‘disorder’’ relation that emerges from a single type of entropy.

The extension of the concept of majorization to quantum density operators is straightforward. Given two density operators ( $\rho \geq 0, \text{Tr } \rho = 1$ ), we say that  $\rho' \prec \rho$  iff its eigenvalue spectrum  $\lambda(\rho')$ , sorted in decreasing order, is majorized by that of  $\rho$ :

$$\rho' \prec \rho \iff \lambda(\rho') \prec \lambda(\rho). \quad (\text{A9})$$

All previous entropic properties remain then valid for operators, replacing  $S(\mathbf{p}) \rightarrow S(\rho)$ . Again, if the corresponding Hilbert space dimensions differ, the definition is applied by padding with zeros the spectrum of lowest dimension. Moreover, Eq. (A3) is generalized to [19]

$$\rho \prec \rho' \iff \rho = \sum_i \gamma_i U_i \rho U_i^\dagger \quad (\text{A10})$$

where  $\{\gamma_i \geq 0\}$  are again a set of probabilities ( $\sum_i \gamma_i = 1$ ) and  $\{U_i\}$  is a set of unitary operators.

Finally, we prove Lemma 1, i.e. the sufficient condition for Eqs. (33)-(35), concerning the system-time entanglement spectrum  $\lambda^{(N)} = \{\lambda_k^{(N)}\}$  of  $|\Psi^{(N)}\rangle$  and  $\lambda^{(N+1)} = \{\frac{N}{N+1} \lambda_k^{(N)}\} \cup \{\frac{1}{N+1}\}$  of  $|\Psi^{(N+1)}\rangle$ , after the addition of a state  $|\psi_n\rangle$  orthogonal to all previous states.

After sorting the eigenvalues in decreasing order, the partial sums  $S_k = \sum_{k'=1}^k \lambda_{k'}$  of  $\lambda^{(N)}$  and  $\lambda^{(N+1)}$  satisfy  $S_k^{(N+1)} = \frac{N}{N+1} S_k^{(N)} \leq S_k^{(N)}$  for  $\lambda_k^{(N)} \geq \frac{1}{N}$ , and  $S_k^{(N+1)} = \frac{N}{N+1} [S_k^{(N)} + \frac{1}{N} - \lambda_k^{(N)}]$  otherwise, again satisfying  $S_k^{(N+1)} \leq S_k^{(N)}$  since  $1 - N\lambda_k^{(N)} \leq S_k^{(N)}$ .  $\square$

## Appendix B: Volatility

Volatility, broadly understood as the degree of variation in asset returns, is a key variable in modern finance due to its impact on derivative pricing, portfolio construction and risk management. Its historical behavior offers valuable insights into the mechanisms governing market dynamics. Empirical studies have documented that volatility is not constant over time, but instead exhibits patterns such as clustering, mean reversion and asymmetric responses to market shocks. These facts, first formalized in models such as the Autoregressive Conditional Heteroskedasticity (ARCH) framework of Engle [62] and its generalized form (GARCH) Bollerslev [63], highlight the importance of analyzing past volatility as a means of understanding and forecasting future uncertainty. These models capture the empirical regularity of volatility clustering: periods of high volatility tend to be followed by high volatility, while those of low volatility tend to be followed by low volatility.

The study of past volatility is not solely of academic interest; it has immediate implications for market participants and policymakers, such as portfolio managers and derivative traders. Regulators and central banks may also rely on historical volatility analysis when designing stress-testing frameworks or assessing systemic risk, as elevated or persistent volatility can signal vulnerabilities in financial stability. In this context, the systematic examination of past volatility serves as both a diagnostic tool for identifying latent risks and a foundation for developing predictive models [64] that inform decision-making across a wide spectrum of financial activities.

Despite decades of research, the analysis of past volatility remains highly relevant in today’s financial landscape. Structural shifts in market microstructure, the proliferation of algorithmic and high-frequency trading (HFT), and the emergence of new asset classes such as cryptocurrencies have altered the dynamics of price formation and volatility transmission. Moreover, periods of extreme market stress, such as the global financial crisis of 2008 or the COVID-19 pandemic, have highlighted the

need for models capable of adapting to rapidly changing environments and capturing non-linear responses.

*Volatility indicators.* The VIX index [41] was introduced by the Chicago Board Options Exchange (CBOE) in 1993. It was originally designed to measure the implied volatility of at-the-money (ATM) SP-100 Index (OEX) option prices for 30 days [65]. The VIX is now based on the S&P500 index (or SPX), the core index for U.S. equities, and estimates expected volatility by averaging

the weighted quotes of SPX put and call options over a wide range of strike prices [66]. The VIX is presently the standard measure of volatility, and it even has ETFs that track its short-term futures, such as the ProShares VIX Short-Term Futures ETF (VIXY). Similarly, the crypto volatility index (CVI), also denoted as “VIX for crypto”, is an index elaborated by a decentralized platform that measures the 30-day implied volatility of Bitcoin (BTC) and Ethereum (ETH) [42].

- 
- [1] D.N. Page and W.K. Wootters, “Evolution without evolution: Dynamics described by stationary observables,” *Phys. Rev. D* **27**, 2885 (1983), W.K. Wootters, “Time replaced by quantum correlations”, *Int. J. Th. Phys.* **23**, 701 (1984).
- [2] V. Giovannetti, S. Lloyd, and L. Maccone, “Quantum time,” *Phys. Rev. D* **92**, 045033 (2015).
- [3] E. Moreva, G. Brida, M. Gramegna, V. Giovannetti, L. Maccone, and M. Genovese, “Time from quantum entanglement: An experimental illustration,” *Phys. Rev. A* **89**, 052122 (2014).
- [4] J.R. McClean, A. Aspuru-Guzik, “Clock quantum Monte Carlo technique: An imaginary-time method for real time quantum dynamics,” *Phys. Rev. A* **91**, 012311 (2015).
- [5] A. Boette, R. Rossignoli, N. Gigena, and M. Cerezo, “System-time entanglement in a discrete-time model,” *Phys. Rev. A* **93**, 062127 (2016).
- [6] A. Boette and R. Rossignoli, “History states of systems and operators,” *Phys. Rev. A* **98**, 032108 (2018).
- [7] E.O. Dias and F. Parisio, “Space-time-symmetric extension of nonrelativistic quantum mechanics,” *Phys. Rev. A* **95**, 032133 (2017).
- [8] A. Nikolova *et al.*, “Relational time in anyonic systems,” *Phys. Rev. A* **97**, 030101(R) (2018).
- [9] P.J. Coles, V. Katariya, S. Lloyd, I. Marvian, and M.M. Wilde, “Entropic energy-time uncertainty relation,” *Phys. Rev. Lett.* **122**, 100401 (2019).
- [10] D. Pabón, L. Rebón, Bordakevich S., Gigena N., Boette A., Iemmi C., Rossignoli R., and Ledesma S, “Parallel-in-time optical simulation of history states,” *Phys. Rev. A* **99**, 062333 (2019).
- [11] F. Lomoc, A. P. Boette, N. Canosa, and R. Rossignoli, “History states of one-dimensional quantum walks,” *Phys. Rev. A* **106**, 062215 (2022).
- [12] N.L. Diaz, P. Braccia, M. Larocca, J. M. Matera, R. Rossignoli, and M. Cerezo, “Parallel-in-time quantum simulation via Page and Wootters quantum time,” *Phys. Rev. Res.* **7**, 033294 (2025).
- [13] Z. Zhao *et al.*, “Geometry of quantum correlations in space-time,” *Phys. Rev. A* **98**, 052312 (2018).
- [14] N. L. Diaz and R. Rossignoli, “History state formalism for Dirac’s theory,” *Phys. Rev. D* **99**, 045008 (2019).
- [15] N. L. Diaz, J. M. Matera, and R. Rossignoli, “History state formalism for scalar particles,” *Phys. Rev. D* **100**, 125020 (2019), “Spacetime quantum actions”, *Phys. Rev. D* **103**, 065011 (2021).
- [16] Giovannetti V., Lloyd S., and Maccone L., “Geometric event based quantum mechanics,” *New J. Phys.* **23**, 023027 (2023).
- [17] N. L. Diaz, J. M. Matera, and R. Rossignoli, “Space-time quantum and classical mechanics with dynamical foliation,” *Phys. Rev. D* **109**, 105008 (2024).
- [18] R. Bhatia, *Matrix Analysis* (Springer, 1997).
- [19] M.A. Nielsen, I.L. Chuang, *Quantum computation and Quantum Information* (Cambridge Univ. Press., 2001).
- [20] F. Black and M. Scholes, “The pricing of options and corporate liabilities,” *J. Pol. Econ.* **81**, 637 (1973).
- [21] R. Merton, “Theory of rational option pricing,” *Bell J. of Economics and Management Science* **4**, 141 (1973).
- [22] R. Elliott and P. Kopp, *Mathematics of financial markets* (Springer Science, 2005).
- [23] S. Shreve, *Stochastic calculus for finance I: the binomial asset pricing model* (Springer Science, 2005).
- [24] M-C. Wu, M-C. Huang, H-C. Yu, and T.C. Chiang, “Phase distribution and phase correlation of financial time series,” *Phys. Rev. E* **73**, 016118 (2006).
- [25] D.J. Fenn, M.A. Porter, S. Williams, M. McDonald, N.F. Johnson, N.S. Jones, “Temporal evolution of financial-market correlations,” *Phys. Rev. E* **84**, 026109 (2011).
- [26] P. Muldowney, *A modern theory of random variation: with applications in stochastic calculus, financial mathematics and Feynman integration* (J. Wiley & Sons, 2013).
- [27] P. Fiedor, “Networks in financial markets based on mutual information rate,” *Phys. Rev. E* **89**, 052801 (2014).
- [28] R.J. Buonocore, T. Aste, and T. Di Matteo, “Asymptotic scaling properties and estimation of the generalized Hurst exponents in financial data,” *Phys. Rev. E* **95**, 042311 (2017).
- [29] M. Schaden, “Quantum finance,” *Physica A* **316**, 511 (2002).
- [30] E. Haven, “A discussion on embedding the Black-Scholes option pricing model in a quantum physics setting,” *Physica A* **304**, 507 (2002).
- [31] Z. Chen, “Quantum theory for the binomial model in finance theory,” *J. Syst. Sci. Complex.* **17** (2004).
- [32] B. Baaquie, *Quantum Finance: Path Integrals and Hamiltonians for Options and Interest Rates* (Cambridge University Press, 2007).
- [33] C. Zhang and L. Huang, “A quantum model for the stock market,” *Physica A* **389**, 5769 (2010).
- [34] M. Contreras, R. Pellicer, M. Villena, and A. Ruiz, “A quantum model of option pricing: When Black-Scholes meets Schrödinger and its semi-classical limit,” *Physica A* **389**, 5447 (2010).
- [35] P. Rebentrost, B. Gupt, and T.R. Bromley, “Quantum computational finance: Monte Carlo pricing of financial derivatives,” *Phys. Rev. A* **98**, 022321 (2018).
- [36] R. Orus, S. Múgel, and E. Lizaso, “Quantum computing for finance: overview and prospects,” *Rev. Phys.* **4**, 100028 (2019).

- [37] D. Orrell, “A quantum model of supply and demand,” *Physica A* **539**, 122928 (2020).
- [38] D. J. Egger *et al.*, “Quantum computing for finance: state-of-the-art and future prospects,” *IEEE Trans. Quantum Eng.* **1**, 3101724 (2020).
- [39] Y. Lu and J. Yang, “Quantum financing system: A survey on quantum algorithms, potential scenarios and open research issues,” *J. Ind. Inf. Integr.* **41**, 100663 (2024).
- [40] S. De Backer, L.E.C. Rocha, R. Ryckebusch, K. Schoors, “On the potential of quantum walks for modeling financial return distributions,” *Physica A* **657**, 130215 (2025).
- [41] R.E. Whaley, “Understanding the VIX,” *J. Portfolio Management* **35**, 98 (2009).
- [42] A.P.N. Nguyen, M. Crane, and M. Bezbradica, “Cryptocurrency volatility index: An efficient way to predict the future CVI,” in *Artificial Intelligence and Cognitive Science*, edited by L. Longo and R. O’Reilly (Springer Nature Switzerland, 2023) p. 355.
- [43] B. DeWitt, “Quantum theory of gravity. I. The canonical theory,” *Phys. Rev.* **160**, 1113 (1967).
- [44] C. Beck and F. Schlögl, *Thermodynamic of Chaotic Systems* (Cambridge Univ. Press, UK, 1993).
- [45] N. Canosa and R. Rossignoli, “Generalized nonadditive entropies and quantum entanglement,” *Phys. Rev. Lett.* **88**, 170401 (2002).
- [46] C. Tsallis, *Introduction to Non-Extensive Statistical Mechanics* (Springer, N.Y., 2009).
- [47] R. Rossignoli and N. Canosa, “Generalized entropic criterion for separability,” *Phys. Rev. A* **66**, 042306 (2002).
- [48] N. Canosa and R. Rossignoli, “Majorization and generalized entropies” in: *Generalized Entropies, Concepts and recent advances in generalized information measures and statistics*, edited by A Kowalski *et al.* (Betham Science Pub., 2013) p. 100.
- [49] R. Rossignoli and N. Canosa, “Violation of majorization relations in entangled states and its detection by means of generalized entropic forms,” *Phys. Rev. A* **67**, 042302 (2003).
- [50] D.F. Walls, and G.J. Milburn, *Quantum Optics* (Springer, 2007).
- [51] E. Schrödinger, “Der stetige übergang von der mikro- zur makromechanik,” *Naturwissenschaften* **14**, 664 (1926).
- [52] R. J. Glauber, “Coherent and incoherent states of the radiation field,” *Phys. Rev.* **131**, 2766 (1963).
- [53] E.C. Sudarshan, “Equivalence of semiclassical and quantum mechanical descriptions of statistical light beams,” *Phys. Rev. Lett.* **10**, 277 (1963).
- [54] Yahoo Finance, “SPDR S&P 500 ETF Trust (SPY) Historical Data,” <http://finance.yahoo.com/quote/SPY/history/> (2024).
- [55] Yahoo Finance, “CBOE Volatility Index (VIX) Historical Data,” <http://finance.yahoo.com/quote/%5EVIX/history/> (2024).
- [56] Yahoo Finance, “Gold (GC=F) Historical Data,” <http://finance.yahoo.com/quote/GOLD/history/>(2024).
- [57] Yahoo Finance, “Bitcoin (BTC-USD) Historical Data,” <http://finance.yahoo.com/quote/BTC-USD/history/> (2024).
- [58] Federal Reserve Bank of St. Louis, “CBOE Gold ETF Volatility Index ,” <http://fred.stlouisfed.org/series/GVZCLS/> (2024).
- [59] Investing.com, “Crypto Volatility Index (CVI),” <http://es.investing.com/indices/crypto-volatility-index-historical-data/> (2025).
- [60] A. Wherl, “General properties of entropy,” *Rev. Mod. Phys.* **50**, 221 (1978).
- [61] R. Rossignoli and N. Canosa, “Non-additive entropies and quantum statistics,” *Phys. Lett. A* **264**, 148 (1999).
- [62] R.F. Engle, “Autoregressive conditional heteroscedasticity with estimates of the variance of united kingdom inflation,” *Econometrica* **50**, 987 (1982).
- [63] T. Bollerslev, “Generalized autoregressive conditional heteroskedasticity,” *J. of Econometrics* **31**, 307 (1986).
- [64] Z. Eisler, J. Perelló, and J. Masoliver, “Volatility: A hidden markov process in financial time series,” *Phys. Rev. E* **76**, 056105 (2007).
- [65] R. E. Whaley, “Derivatives on market volatility,” *J. Deriv.* **1**, 71 (1993).
- [66] J. Osterrieder, L. Vetter, and K. Röschli, “The VIX volatility index—A very thorough look at it,” SSRN ELibrary , 3311727 (2019).